Journal of Translational Gastroenterology **2026** | Epub
DOI: 10.14218/JTG.2026.00029

Original Article

17β-Estradiol Attenuates Hypoxia-induced Lipid Accumulation in Hepatocytes *in vitro* and Is Associated with Changes in Oxidative Stress and Mitochondrial Quality Control

Jin-Hong Liu[1#], Ning-Lin Wu[1#], Yu-Jie Yang[2,3], Jing-Dan Weng[2], Li-Ping Chen[2], Jia-Cheng Xian[2], Yu-Hang Xiang[2], Yuan-Yuan Zhang[2,3] and Xiao-Dong Sun[1,2*]

[1]*The Medical College, Xizang University, Lhasa, Xizang, China;* [2]*Department of Pharmacology, West China School of Basic Medical Sciences & Forensic Medicine, West China School of Pharmacy, Sichuan University, Chengdu, Sichuan, China;* [3]*West China Lecheng Hospital of Sichuan University, Qionghai, Hainan, China*

[#]*These authors contributed equally to this work.*

Received: August 08, 2026 | **Revised:** October 15, 2026 | **Accepted:** November 11, 2026 | **Published online:** November 24, 2026

Abstract

Background and objectives: Hypoxia disrupts hepatic lipid metabolism and mitochondrial homeostasis. This study aimed to investigate whether 17β-estradiol (E2) attenuates hypoxia-induced lipid accumulation in hepatocytes *in vitro* and examine associated oxidative and mitochondrial quality control (MQC) responses.

Methods: Huh-7 and AML12 cells were exposed to normoxia (21% O_2) or hypoxia (1% O_2) with or without E2 (10 nM). Lipid accumulation and dihydroethidium (DHE) fluorescent signals were assessed by Oil Red O/Nile Red and DHE staining, respectively. MitoTimer, western blotting, TOMM20 immunofluorescence, and mitochondrial–lysosomal colocalization were used to evaluate MQC-related changes. Stable *PRKN*-knockdown Huh-7 cells and chloroquine treatment were used for functional analysis.

Results: E2 reduced hypoxia-induced lipid accumulation and DHE fluorescent signals and increased antioxidant protein expression. E2 was associated with improved mitochondrial protein turnover-related signals, increased expression of mitochondrial biogenesis-related proteins, and improved mitochondrial network morphology with corresponding changes in optic atrophy 1, mitofusin 1, and dynamin-related protein 1. E2 also altered E3 ubiquitin-protein ligase Parkin phosphorylation and the expression of mitophagy-related proteins. *PRKN* silencing attenuated the E2-associated increase in mitochondrial–lysosomal colocalization and significantly modified the responses of lipid accumulation and DHE fluorescent signals to E2 under hypoxia.

Conclusions: E2 attenuates hypoxia-induced lipid accumulation and DHE fluorescent signals in hepatocytes *in vitro* and is associated with improved MQC responses. *PRKN* silencing alters several E2-associated responses, supporting the involvement of *PRKN*-related processes.

Keywords: Hypoxia; Hepatic lipid accumulation; 17β-Estradiol; Estrogen; Oxidative stress; Mitochondrial quality control.
***Correspondence to:** Xiao-Dong Sun, Department of Pharmacology, West China School of Basic Medical Sciences & Forensic Medicine, West China School of Pharmacy, Sichuan University, Chengdu, Sichuan 610041, China. ORCID: https://orcid.org/0000-0002-7062-8931. Tel: +86-28-8550-1278, E-mail: sunxd@scu.edu.cn
How to cite this article: Liu JH, Wu NL, Yang YJ, Weng JD, Chen LP, Xian JC, *et al*. 17β-Estradiol Attenuates Hypoxia-induced Lipid Accumulation in Hepatocytes *in vitro* and Is Associated with Changes in Oxidative Stress and Mitochondrial Quality Control. *J Transl Gastroenterol*. Published online: Nov 24, 2026. DOI: 10.14218/JTG.2026.00029.

Introduction

The liver is highly sensitive to hypoxia.[1] Experimental evidence indicates that chronic hypoxia can alter hepatic lipid metabolism and increase hepatic lipid accumulation in rats.[2] Metabolic dysfunction-associated steatotic liver disease (MASLD; formerly termed nonalcoholic fatty liver disease) has become the most common chronic liver disease worldwide, with a global prevalence

© 2026 The Author(s). This article has been published under the terms of Creative Commons Attribution-Noncommercial 4.0 International License (CC BY-NC 4.0), which permits noncommercial unrestricted use, distribution, and reproduction in any medium, provided that the following statement is provided. "This article has been published in *Journal of Translational Gastroenterology* at https://doi.org/10.14218/JTG.2026.00029 and can also be viewed on the Journal's website at https://www.xiahepublishing.com/journal/jtg".

that has reached 32.4% and has continued to rise in recent years.[3,4]

Dysregulated hepatic lipid metabolism is the core pathological mechanism underlying excessive lipid accumulation in hepatocytes induced by hypoxia. Under hypoxia, this dysregulation leads to abnormal lipid accumulation, resulting in overproduction of reactive oxygen species (ROS) that induce oxidative stress and hepatocyte dysfunction.[5,6] Mitochondria are the primary sites of adenosine triphosphate and ROS production in cells. Proper lipid metabolism and redox homeostasis are essential for maintaining mitochondrial structure and function, as disrupted lipid trafficking and lipotoxicity impair mitochondrial integrity and trigger oxidative stress.[7] Oxidative stress from excessive lipid accumulation impairs mitochondrial function, which in turn exacerbates lipid metabolic abnormalities, creating a vicious cycle.[8] Mitochondrial quality control (MQC) plays a key role in maintaining mitochondrial homeostasis by clearing damaged mitochondria, promoting mitochondrial biogenesis, and improving the mitochondrial network structure.[9,10] Accordingly, mitochondria have emerged as potential therapeutic targets across multiple diseases, supporting therapeutic strategies aimed at restoring mitochondrial homeostasis.[11]

The prevalence of MASLD exhibits sexual dimorphism, with men having a significantly higher prevalence than women, and this difference manifests differently across various age groups. In particular, the prevalence among premenopausal women is significantly lower than that among postmenopausal women.[12,13] A key contributor to these differences is estrogen, whose primary form in the human body is 17β-estradiol (E2).[14] Estrogen maintains mitochondrial structure and functional homeostasis by regulating MQC and inhibiting ROS overproduction.[15] Estrogen also promotes mitochondrial biogenesis, upregulates proteins associated with mitochondrial fusion to support mitochondrial dynamics, and enhances mitophagy to clear damaged mitochondria.[16-18] However, it remains unclear whether E2 alleviates hypoxia-induced lipid accumulation in hepatocytes and whether this effect is associated with changes in oxidative stress and MQC. We established *in vitro* hypoxia-induced lipid accumulation models using Huh-7 and AML12 cells to investigate E2's effects and potential mechanisms in hypoxia-induced hepatic lipid accumulation.

Materials and methods

Cell culture and establishment of a hypoxia-induced lipid accumulation model

Huh-7 and AML12 cells were purchased from Haixing Biotechnology (Suzhou, China). Huh-7 cells were maintained in Dulbecco's modified Eagle medium (DMEM; BasalMedia, Shanghai, China), whereas AML12 cells were cultured in Dulbecco's modified Eagle medium/nutrient mixture F-12 (DMEM/F-12; BasalMedia, Shanghai, China). Both culture media were supplemented with 10% fetal bovine serum (FBS) and 1% penicillin–streptomycin (HyClone, Logan, UT, USA). No additional insulin, transferrin, selenium, or dexamethasone was added to the AML12 culture medium. Phenol-red-free medium and charcoal-stripped FBS were not used. Cells were maintained in a humidified incubator at 37°C with 5% CO_2.

E2 (Aladdin, Shanghai, China) was dissolved in dimethyl sulfoxide (DMSO; BBI, Shanghai, China) to prepare a stock solution, which was subsequently diluted into the culture medium to a working concentration of 10 nM. This concentration was determined based on our laboratory's experience and relevant reports.[19,20] The final DMSO concentration in all treatment groups was maintained at 0.1% (v/v).

The hypoxia-induced lipid accumulation model was established using a hypoxia chamber (Billups-Rothenberg Inc., Del Mar, CA, USA) placed in a cell culture incubator (Thermo Fisher Scientific, Waltham, MA, USA). Cells were maintained under hypoxic conditions (1% O_2, 5% CO_2, and 94% N_2). Cells were divided into four experimental groups: Normoxia (21% O_2), Normoxia + E2 (21% O_2 with 10 nM E2), Hypoxia (1% O_2), and Hypoxia + E2 (1% O_2 with 10 nM E2). Cells in the Normoxia group were cultured under 21% O_2 for 48 h. For the Normoxia + E2 group, cells were cultured under 21% O_2 for 24 h, followed by treatment with 10 nM E2 for another 24 h under 21% O_2. Cells in the Hypoxia group were incubated under 1% O_2 for 48 h. For the Hypoxia + E2 group, cells were first exposed to 1% O_2 for 24 h and then treated with 10 nM E2 for an additional 24 h under 1% O_2.

Oil Red O staining assay

The following Oil Red O staining assay was performed in AML12 hepatocytes. Oil Red O powder (BBI, Shanghai, China) was dissolved in isopropanol to prepare a 0.5% stock solution. A 0.3% Oil Red O working solution was freshly prepared by mixing the stock solution with ultrapure water at a 3:2 volume ratio. Cells were washed twice with phosphate-buffered saline (PBS) and fixed with 4% paraformaldehyde (Aladdin, Shanghai, China; prepared in-house as a 4% solution in PBS) for 20 min at room temperature. Then, cells were rinsed with PBS and stained with the Oil Red O working solution for 45 min at room temperature. Nuclei were counterstained with hematoxylin (BBI, Shanghai, China; prepared from powder) for 5 min, then blued with 10 mM Tris solution (prepared from Tris powder; BBI, Shanghai, China) for 3 min.[21] After washing with ultrapure water, the slides were mounted with glycerol, and images were captured using an AxioScope A1 microscope (Carl Zeiss, Oberkochen, Germany).

Nile Red staining assay

The following Nile Red staining assay was performed in AML12 and Huh-7 hepatocytes. Nile Red powder (BBI, Shanghai, China) was dissolved in DMSO to prepare a 30 mM stock solution, then diluted into serum-free DMEM/F-12 or DMEM to a final working concentration of 5 μM. After the indicated treatment, cells were incubated with the Nile Red working solution at 37°C in the dark for 30 min. The nuclei were then counterstained with Hoechst 33258 (Sigma, Missouri, USA) for 10 min at room temperature in the dark. After staining, the cells were washed with PBS, then ultrapure water, and mounted in an antifade mounting medium. Fluorescence images were captured using an Axio Observer 7 microscope (Carl Zeiss, Oberkochen, Germany).

Dihydroethidium staining

The following dihydroethidium (DHE) staining assay was performed in AML12 and Huh-7 hepatocytes. DHE powder (MedChemExpress, New Jersey, USA) was dissolved in DMSO to prepare a 10 mM stock solution, then diluted into serum-free DMEM/F-12 or DMEM to a final working concentration of 15 μM. Following the indicated treatment, cells were washed with

PBS and incubated with the DHE working solution at 37°C for 30 min. Then, cells were washed with PBS, and serum-free DMEM/F-12 or DMEM was added before the cells were immediately imaged on an Axio Observer 7 microscope (Carl Zeiss, Oberkochen, Germany) at 488 nm excitation and 611 nm emission. DHE fluorescence intensity was quantified using ImageJ (National Institutes of Health, Bethesda, Maryland, USA).

MitoTimer fluorescence assay

The MitoTimer lentiviral particles used in this study were purchased from OBiO (Shanghai, China). Huh-7 cells were seeded in six-well plates at 6×10^5 cells per well. Upon reaching 70% confluence, cells were transduced with MitoTimer lentiviral particles at a multiplicity of infection of 0.1 for 48 h. The infected cells were then passaged at a 1:6 ratio and cultured in six-well plates. After 24 h, stable cell lines were selected with 2 μg/mL puromycin for 24 h. Cells exhibiting nearly 100% positive fluorescence were expanded in 10 cm culture dishes for subsequent experiments.

Stably transduced Huh-7 cells were divided into four experimental groups: Normoxia (21% O_2), Normoxia + E2 (21% O_2 with 10 nM E2), Hypoxia (1% O_2), and Hypoxia + E2 (1% O_2 with 10 nM E2). For the E2 intervention groups, cells were first cultured under normoxia or hypoxia for 24 h, then treated with 10 nM E2, and incubated under the same oxygen conditions for another 24 h. Cells were then washed with PBS and fixed with 4% paraformaldehyde for 20 min at room temperature in the dark. Cells were then permeabilized with 0.5% Triton X-100 (BBI, Shanghai, China) for 15 min and blocked with 4% bovine serum albumin (Neofroxx, Einhausen, Germany) for 1 h at room temperature. Nuclei were stained with Hoechst 33258 in PBS for 10 min. After washing, the samples were mounted with an antifade mounting medium. Images were acquired using a Zeiss LSM 710 confocal laser-scanning microscope (Carl Zeiss, Oberkochen, Germany), and fluorescence intensity was quantified using ImageJ.

TOMM20 immunofluorescence and mitochondrial network analysis

Huh-7 cells were seeded on glass coverslips and treated as indicated. Following treatment, cells were washed three times with PBS and fixed with 4% paraformaldehyde for 15 min at room temperature. Cells were permeabilized with 0.1% Triton X-100 for 10 min and blocked with 5% bovine serum albumin for 1 h. Then, cells were incubated overnight at 4°C with an anti-TOMM20 primary antibody (Proteintech, Wuhan, China, Cat. No. 11802-1-AP, 1:200), followed by incubation with an Alexa Fluor 647-conjugated goat anti-rabbit immunoglobulin G (IgG; heavy and light chains [H+L]) secondary antibody (Jackson ImmunoResearch, West Grove, PA, USA, Cat. No. 111-605-003, 1:3000) for 1 h at room temperature in the dark. Nuclei were counterstained with Hoechst 33258. Images were acquired using a confocal laser scanning microscope (Zeiss LSM 710; Carl Zeiss, Oberkochen, Germany).

Mitochondrial morphology and network organization were analyzed using the Analyze Skeleton (2D/3D) plugin in Fiji (National Institutes of Health, Bethesda, Maryland, USA). TOMM20 fluorescence images were processed to generate binary masks and skeletonized mitochondrial network structures. The perinuclear-to-peripheral fluorescence intensity ratio and mean branch length were quantified to assess mitochondrial distribution and network morphology, respectively. For each independent experiment, five randomly selected fields were analyzed, with approximately one or two cells analyzed per field, resulting in approximately 5–10 cells analyzed per group. The measurements from individual cells within each independent experiment were averaged to generate one value for that biological replicate, and the three independent biological replicates were used for statistical analysis. Image acquisition, field selection, and image quantification were performed with the investigators blinded to the experimental groups.

Lentivirus-mediated PRKN knockdown

Lentiviral vectors carrying short hairpin RNA targeting *PRKN* (sh*PRKN*; target sequence CUUGGCUACUCCCUGCCUU) and the corresponding non-targeting control lentivirus (shNC) were purchased from OBiO (Shanghai, China). Huh-7 cells were routinely cultured, seeded at a 1:10 dilution in six-well plates, and maintained at 37°C with 5% CO_2. After 24 h, the culture medium was replaced with lentivirus-containing medium, and lentiviral infection was performed at a multiplicity of infection of 20. Following infection, puromycin (Sangon, Shanghai, China) was added at a final concentration of 2 μg/mL to select stably transduced cells.

Two stable Huh-7 cell lines were generated after puromycin selection: shNC (non-targeting control) and sh*PRKN* (*PRKN* knockdown). The shNC cell line was used together with sh*PRKN* for assessment of lipid accumulation and DHE fluorescent signals using Nile Red and DHE staining, respectively. For the subsequent mitophagy-related immunofluorescence assay with chloroquine (CQ) treatment, both the shNC and sh*PRKN* stable cell lines were also included. The efficiency of *PRKN* knockdown was confirmed by western blotting of Parkin expression before functional experiments.

Immunofluorescence assessment of mitophagy-related activity following CQ treatment

Stable Huh-7-shNC and Huh-7-sh*PRKN* cells were seeded on glass coverslips in 24-well plates. After attachment, cells were transiently transfected with pEGFP-N1-LAMP1, which encodes LAMP1 fused to EGFP at its C-terminus (LAMP1-GFP), using Lipofectamine 3000 (Thermo Fisher Scientific, Cat. No. L3000015). A single transfection mixture was prepared for 30 wells. Solution A contained 7.5 μL Lipofectamine 3000 diluted in 250 μL serum-free DMEM, and solution B contained 5 μg plasmid DNA and 10 μL P3000 reagent diluted in 250 μL serum-free DMEM. The two solutions were incubated separately for 5 min at room temperature, combined, and incubated for a further 15 min before being added to the cells. The medium was replaced with fresh serum-containing DMEM 6 h after transfection. Subsequent experimental treatments were initiated 24 h after transfection. For shNC cells, four experimental groups were established under normoxia (21% O_2) or hypoxia (1% O_2): Normoxia, Normoxia + E2 (10 nM), Hypoxia, Hypoxia + E2 (10 nM). Six additional experimental groups comprising stable shNC and sh*PRKN* cells were established under hypoxia (1% O_2): sh*PRKN*, sh*PRKN* + E2 (10 nM), shNC + CQ, shNC + CQ + E2 (10 nM), sh*PRKN* + CQ, sh*PRKN* + CQ + E2 (10 nM). CQ (10 μM) was added during the final 6 h of hypoxia before fixation to inhibit lysosomal

degradation.

After treatment, cells were subjected to immunofluorescence staining for TOMM20 with 4′,6-diamidino-2-phenylindole nuclear counterstaining as described above. Coverslips were mounted on glass slides. Images were acquired using a Zeiss LSM 710 confocal laser-scanning microscope (Carl Zeiss, Oberkochen, Germany), and fluorescence intensity and mitochondrial–lysosomal colocalization were quantified in ImageJ.

Western blotting

Total proteins were extracted using cell lysis buffer containing 2% (w/v) sodium dodecyl sulfate (SDS; prepared from a 10% (w/v) stock solution; Aladdin, China). Total protein concentrations were determined using a BCA protein assay kit (Beyotime, China, Cat. No. P0010S) with bovine serum albumin as the standard. Protein samples were denatured at 98°C for 10 min and centrifuged at 12,000 × *g* for 3 min. Equal amounts of total protein (13.6 μg per lane) were separated by SDS-polyacrylamide gel electrophoresis and transferred onto polyvinylidene fluoride membranes (Merck, Darmstadt, Germany). The membranes were blocked with 5% skim milk in Tris-buffered saline containing Tween 20 (TBST; BBI, Shanghai, China) for 1 h at room temperature, then incubated overnight at 4°C with the primary antibodies. After washing with TBST, membranes were incubated with the horseradish peroxidase (HRP)-conjugated secondary antibodies for 1 h at room temperature. Bands were visualized using an ultrasensitive enhanced chemiluminescence reagent (BBI, Shanghai, China) and imaged with a chemiluminescence imaging system (Clinx, Shanghai, China). Band intensities were quantified using ImageJ and normalized to the corresponding loading control. β-actin, β-tubulin, or GAPDH was selected according to its molecular mass relative to the target protein, allowing the target protein and loading control to be detected on the same membrane. These loading controls showed stable expression under their respective experimental conditions.

The primary antibodies (Table 1) used in this study included anti-β-tubulin (Biodragon, Chengdu, China), anti-β-actin (Santa Cruz, Texas, USA), anti-GAPDH (Biodragon, Chengdu, China), anti-HIF-1α (BBI, Shanghai, China), anti-SOD1 (Proteintech, Wuhan, China), anti-SOD2 (Proteintech, Wuhan, China), anti-NQO1 (BBI, Shanghai, China), anti-TFAM (Proteintech, Wuhan, China), anti-PGC-1α (Proteintech, Wuhan, China), anti-NRF1 (Proteintech, Wuhan, China), anti-MFN1 (Proteintech, Wuhan, China), anti-OPA1 (Abclonal, Wuhan, China), anti-DRP1 (BBI, Shanghai, China), anti-p-Parkin (Bioss, Beijing, China), anti-Parkin (Bioss, Beijing, China), anti-SQSTM1 (Proteintech, Wuhan, China), and anti-LC3B (MBL Life Science, Nagoya, Japan). HRP-conjugated goat anti-rabbit IgG (H+L) and goat anti-mouse IgG (H+L) secondary antibodies (Thermo Fisher, Massachusetts, USA) were used as the secondary antibodies (Table 2).

Statistical analysis

Statistical analyses were performed using GraphPad Prism 10 (GraphPad Software, Boston, Massachusetts, USA, www.graphpad.com). Data are presented as the mean ± standard deviation. Three independent biological replicates ($n = 3$) were performed for each experiment, with each biological replicate representing an independently performed experiment involving separate cell seeding, treatment, and sample processing. For Oil Red O staining, images were acquired using a 20× objective. Each group included two technical replicate wells in each independent biological replicate, and three randomly selected microscopic fields were analyzed from each technical replicate well. Lipid droplet area was normalized to the total number of cells in the corresponding field, with approximately 150 cells analyzed per group in each independent biological replicate. For DHE staining, images were acquired using a 20× objective, and approximately 50–100 cells were analyzed per group in each independent biological replicate. For Nile Red staining, TOMM20 immunofluorescence, MitoTimer fluorescence imaging, and mitochondrial–lysosomal colocalization analysis, images were acquired using a 63× objective. Five randomly selected microscopic fields were examined per group in each independent biological replicate. For the Nile Red assay shown in Figure 1a–c, two or three cells were quantified per field, yielding approximately 10–15 cells per group per biological replicate. For the other assays, approximately one or two cells were examined per field, yielding approximately 5–10 cells per group per biological replicate. Two-group comparisons were performed using an unpaired, two-tailed Student's t-test. Comparisons among multiple groups in single-factor experiments were performed using one-way analysis of variance (ANOVA) followed by Tukey's multiple-comparisons test. For the experiments assessing the effects of *PRKN* knockdown on E2 responses under hypoxia, two-way ANOVA was performed with *PRKN* status (shNC *vs.* sh*PRKN*) and E2 treatment (E2− *vs.* E2+) as the two factors, including the *PRKN* status × E2 treatment interaction. When appropriate, multiple comparisons were performed using Tukey's multiple-comparisons test. For two-way ANOVA, F statistics with numerator and denominator degrees of freedom, P values, and partial η^2 effect sizes [partial $\eta^2 = SS_{effect} / (SS_{effect} + SS_{error})$] were reported for both main effects and their interactions. $P < 0.05$ was considered statistically significant.

Results

Hypoxia increased HIF-1α expression in Huh-7 cells, whereas E2 attenuated hypoxia-induced lipid accumulation in AML12 cells

As shown in Figure 2a, b, HIF-1α expression in Huh-7 cells significantly increased after 24 h of hypoxia compared with the Normoxia group (0 h) ($P < 0.05$). HIF-1α expression in Huh-7 cells at 48 h was similar to that at 24 h, indicating relatively stable HIF-1α expression between 24 and 48 h.

As shown in Figure 2c, d, Oil Red O staining and quantitative analysis showed that AML12 cells in the Hypoxia group had a greater lipid droplet area per cell than those in the Normoxia group ($P < 0.001$), suggesting increased lipid accumulation under hypoxia. Compared with the Normoxia group, the Normoxia + E2 group showed a slight increase in lipid accumulation, less pronounced than the increase under hypoxia, suggesting that E2 had a relatively limited effect on lipid accumulation under normoxia. Compared with the Hypoxia group, the Hypoxia + E2 group showed reduced lipid accumulation ($P < 0.01$), suggesting that E2 treatment attenuated the increase in lipid accumulation under hypoxia.

Nile Red staining and quantitative analysis further showed that

 DOI: 10.14218/JTG.2026.00029 | 2026

Table 1. Primary antibodies used for western blotting

Antibody target	Manufacturer	Catalog no.	Working dilution
β-actin	Santa Cruz	sc-47778	1:3000
β-tubulin	Biodragon	B1031	1:3000
GAPDH	Biodragon	B3029	1:3000
HIF-1α	BBI	D262108	1:1000
SOD1	Proteintech	10269-1-AP	1:3000
SOD2	Proteintech	24127-1-AP	1:3000
NQO1	BBI	D261049	1:3000
TFAM	Proteintech	22586-1-AP	1:3000
PGC-1α	Proteintech	10268-1-AP	1:2000
NRF1	Proteintech	66832-1-Ig	1:3000
MFN1	Proteintech	13798-1-AP	1:5000
OPA1	Abclonal	A9833	1:3000
DRP1	BBI	D198957	1:3000
p-Parkin	Bioss	bs-19882R	1:1000
Parkin	Bioss	bs-23687R	1:4000
SQSTM1	Proteintech	18420-1-AP	1:3000
LC3B	MBL	m186-3	1:3000

DRP1, dynamin-related protein 1; GAPDH, glyceraldehyde-3-phosphate dehydrogenase; HIF-1α, hypoxia-inducible factor 1α; LC3B, microtubule-associated protein light chain 3B; MFN1, mitofusin 1; NQO1, NAD(P)H:quinone oxidoreductase 1; NRF1, nuclear respiratory factor 1; OPA1, optic atrophy 1; PGC-1α, peroxisome proliferator-activated receptor γ coactivator 1α; p-Parkin, phosphorylated Parkin; SOD1, superoxide dismutase 1; SOD2, superoxide dismutase 2; SQSTM1, sequestosome 1; TFAM, mitochondrial transcription factor A.

Table 2. Secondary antibodies used for western blotting

Antibody target	Manufacturer	Catalog no.	Working dilution
Goat anti-rabbit IgG (H+L), HRP	Invitrogen	A16096	1:3000
Goat anti-mouse IgG (H+L), HRP	Invitrogen	62-6520	1:3000

H+L, heavy and light chains; HRP, horseradish peroxidase; IgG, immunoglobulin G.

intracellular lipid accumulation was significantly higher in the Hypoxia group than in the Normoxia group in AML12 cells ($P < 0.001$). Compared with the Normoxia group, the Normoxia + E2 group showed a slight increasing trend in intracellular lipid accumulation. Compared with the Hypoxia group, the Hypoxia + E2 group showed decreased intracellular lipid accumulation ($P < 0.001$), suggesting that E2 treatment reduced intracellular lipid accumulation under hypoxia (Fig. 2e, f).

Overall, hypoxia increased lipid accumulation in AML12 cells, whereas E2 treatment reduced it.

E2 attenuated DHE-detectable fluorescent signals and increased antioxidant protein expression under hypoxia

As shown in Figure 3a, b, DHE staining and quantitative analysis in AML12 cells showed that DHE-detectable fluorescence was significantly increased in the Hypoxia group compared with the Normoxia group ($P < 0.001$), suggesting enhanced DHE fluorescence signals under hypoxia. Compared with the Normoxia group, the Normoxia + E2 group showed an increasing trend in DHE fluorescence. However, the magnitude of change was lower than that observed under hypoxia, suggesting that E2 had a relatively limited effect on DHE-detectable fluorescence under normoxia. Compared with the Hypoxia group, the Hypoxia + E2 group showed decreased fluorescence ($P < 0.001$), suggesting that E2 treatment reduced the enhanced DHE fluorescent signals under hypoxia.

As shown in Figure 3c–f, western blotting and quantitative analysis in Huh-7 cells showed that the expression of the antioxidant proteins NQO1 ($P < 0.001$), SOD1 ($P < 0.05$), and SOD2 ($P < 0.001$) significantly decreased in the Hypoxia group compared with the Normoxia group. Compared with the Normoxia group, the Normoxia + E2 group showed mild changes in the expression of these antioxidant proteins. Compared with the Hypoxia group, the Hypoxia + E2 group showed significantly increased protein expression of NQO1 ($P < 0.01$), SOD1 ($P < 0.001$), and SOD2 ($P < 0.001$).

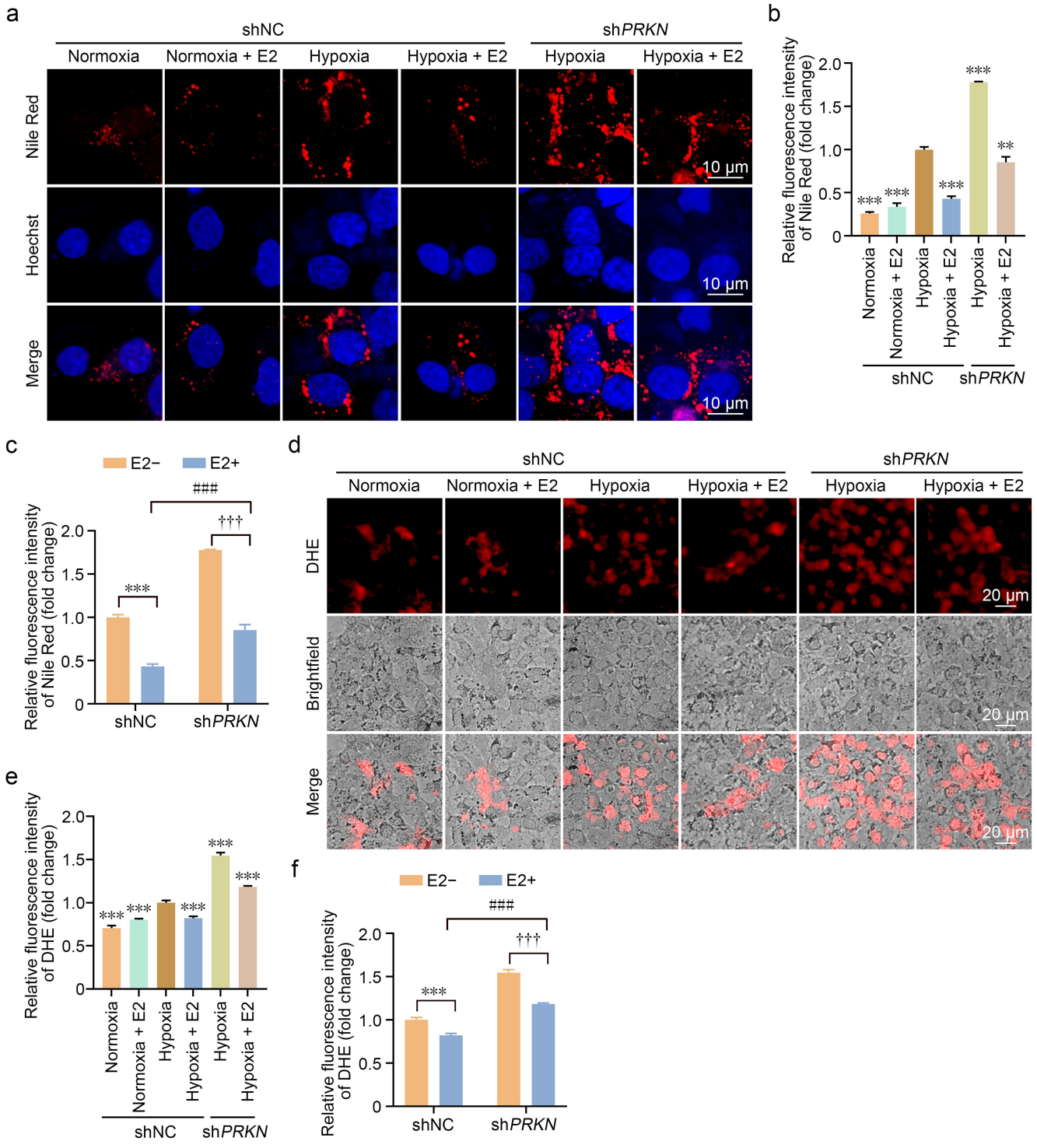


Fig. 1. *PRKN* silencing modified the effects of E2 on hypoxia-induced lipid accumulation and DHE fluorescent signals in Huh-7 cells. Huh-7 cells were used. Cells were divided into shNC and sh*PRKN* groups. The shNC group contained four subgroups: Normoxia (21% O_2), Normoxia + E2, Hypoxia (1% O_2), Hypoxia + E2. The sh*PRKN* group included two hypoxic subgroups: Hypoxia, Hypoxia + E2. The sh*PRKN* group was transduced with lentivirus and subjected to antibiotic selection to generate stable *PRKN* knockdown cell lines. The shNC group was transduced with a negative-control lentivirus and subjected to the same antibiotic selection. Afterward, both cell populations were incubated under normoxia or hypoxia for 24 h. E2 (10 nM) was then added, and cells

 DOI: 10.14218/JTG.2026.00029 | 2026

were further incubated for another 24 h under the same oxygen conditions. (a–c) Intracellular lipid accumulation was detected by Nile Red fluorescence staining. Nile Red images were acquired under a 63× objective lens. Biological replicates, $n = 3$. In each independent biological experiment, five random fields were captured per group; two or three cells were analyzed per field, yielding approximately 10–15 cells per group per biological replicate. Scale bar = 10 μm. Statistical analysis for (b) was performed using one-way ANOVA followed by Tukey's multiple-comparisons test for comparisons among the single-factor treatment groups. $^{**}P < 0.01$, $^{***}P < 0.001$, compared with the Hypoxia + shNC group. Statistical analysis for (c) was performed using two-way ANOVA with *PRKN* status and E2 treatment as the two factors, followed by Tukey's multiple-comparisons test. A significant *PRKN* status × E2 treatment interaction was detected ($P < 0.001$). $^{***}P < 0.001$, shNC E2+ *vs.* shNC E2−; $\dagger\dagger\dagger P < 0.001$, sh*PRKN* E2+ *vs.* sh*PRKN* E2−; $\#\#\#P < 0.001$, sh*PRKN* E2+ *vs.* shNC E2+. (d–f) DHE fluorescence signals were detected by DHE staining. DHE images were acquired under a 20× objective lens. Biological replicates, $n = 3$. A total of 50–100 cells were analyzed for each group owing to high cell density within a single field at this magnification. Scale bar = 20 μm. (e, f) Quantification of relative DHE fluorescence intensity. Statistical analysis for (e) was performed using one-way ANOVA followed by Tukey's multiple-comparisons test for comparisons among the single-factor treatment groups. $^{**}P < 0.01$, $^{***}P < 0.001$, compared with the Hypoxia + shNC group. Statistical analysis for (f) was performed using two-way ANOVA with *PRKN* status and E2 treatment as the two factors, followed by Tukey's multiple-comparisons test. A significant *PRKN* status × E2 treatment interaction was detected ($P = 0.0002$). $^{***}P < 0.001$, shNC E2+ *vs.* shNC E2−; $\dagger\dagger\dagger P < 0.001$, sh*PRKN* E2+ *vs.* sh*PRKN* E2−; $\#\#\#P < 0.001$, sh*PRKN* E2+ *vs.* shNC E2+. Data are presented as the mean ± SD. ANOVA, analysis of variance; DHE, dihydroethidium; E2, 17β-estradiol; *PRKN*, parkin RBR E3 ubiquitin protein ligase gene; SD, standard deviation; shNC, non-targeting control short hairpin RNA; sh*PRKN*, short hairpin RNA targeting *PRKN*.

These results suggested that hypoxia was associated with increased DHE-detectable fluorescent signals in AML12 cells and decreased expression of the antioxidant proteins NQO1, SOD1, and SOD2 in Huh-7 cells. Under hypoxia, E2 treatment reduced DHE-detectable fluorescence and increased expression of these antioxidant proteins.

E2 was associated with changes in mitochondrial protein turnover-related signals and mitochondrial biogenesis-related markers under hypoxia

MitoTimer fluorescence imaging showed that green fluorescence was markedly decreased in Huh-7 cells under hypoxia compared with the Normoxia group. In contrast, red fluorescence changed slightly, resulting in a significantly lower green/red fluorescence ratio ($P < 0.001$). Compared with the Normoxia group, the Normoxia + E2 group also showed a slight decrease in green fluorescence and the green/red fluorescence ratio. Compared with the Hypoxia group, the Hypoxia + E2 group showed significantly increased green fluorescence and green/red fluorescence ratio ($P < 0.001$, Fig. 4a, b). The MitoTimer green/red fluorescence ratio reflects the relative proportion of newly synthesized versus older/matured mitochondrially targeted reporter protein during mitochondrial protein turnover. These results suggested that hypoxia decreased the relative proportion of newly synthesized versus older/matured mitochondrially targeted reporter protein, whereas E2 treatment attenuated this effect.

As shown in Figure 4c–g, these experiments were performed in Huh-7 cells. Western blotting further showed that the expression of TFAM ($P < 0.01$) and NRF1 ($P < 0.001$) significantly decreased in the Hypoxia group compared with the Normoxia group. Compared with the Normoxia group, the Normoxia + E2 group showed reduced expression of these proteins, although the reduction was less pronounced than under hypoxia. Compared with the Hypoxia group, the Hypoxia + E2 group showed significantly increased expression of PGC-1α, TFAM, and NRF1 (PGC-1α and NRF1, $P < 0.001$; TFAM, $P < 0.05$). These results suggested that hypoxia was associated with decreased expression of mitochondrial biogenesis-related proteins, whereas E2 treatment attenuated these changes.

E2 was associated with improved mitochondrial network morphology and changes in mitochondrial dynamics-related proteins under hypoxia

As shown in Figure 5a–d, these experiments were performed in Huh-7 cells. Western blotting showed that expression levels of the mitochondrial dynamics-related proteins OPA1, MFN1, and DRP1 decreased under hypoxia. Compared with the Normoxia group, the Normoxia + E2 group showed a slight decrease in the expression of OPA1, MFN1, and DRP1, suggesting that E2 altered mitochondrial dynamics-related protein expression under normoxia. Compared with the Hypoxia group, the Hypoxia + E2 group showed significantly increased OPA1 ($P < 0.001$) and MFN1 ($P < 0.001$) expression, along with decreased DRP1 expression ($P < 0.001$).

Further TOMM20 immunofluorescence staining and quantitative analysis in Huh-7 cells showed that the perinuclear-to-peripheral TOMM20 fluorescence intensity ratio was significantly increased in the Hypoxia group compared with the Normoxia group ($P < 0.001$). At the same time, mitochondrial mean branch length decreased significantly ($P < 0.001$), indicating changes in mitochondrial network morphology under hypoxia (Fig. 5e–g). Compared with the Normoxia group, the Normoxia + E2 group showed a decreasing trend in the perinuclear-to-peripheral TOMM20 fluorescence intensity ratio and a modest increase in mitochondrial mean branch length. Compared with the Hypoxia group, the Hypoxia + E2 group showed a reduced perinuclear-to-peripheral TOMM20 fluorescence intensity ratio ($P < 0.01$) and a significant increase in mitochondrial mean branch length ($P < 0.001$). These changes in mitochondrial dynamics-related proteins were accompanied by reduced perinuclear accumulation of TOMM20-stained mitochondria and increased mitochondrial mean branch length, suggesting that E2 treatment was associated with improved mitochondrial network organization under hypoxia.

E2 was associated with altered Parkin phosphorylation and mitophagy-related protein expression under hypoxia

As shown in Figure 6a–d, these experiments were performed in Huh-7 cells. Western blot analysis revealed differences in Parkin and its Ser65 phosphorylation levels among the three groups.

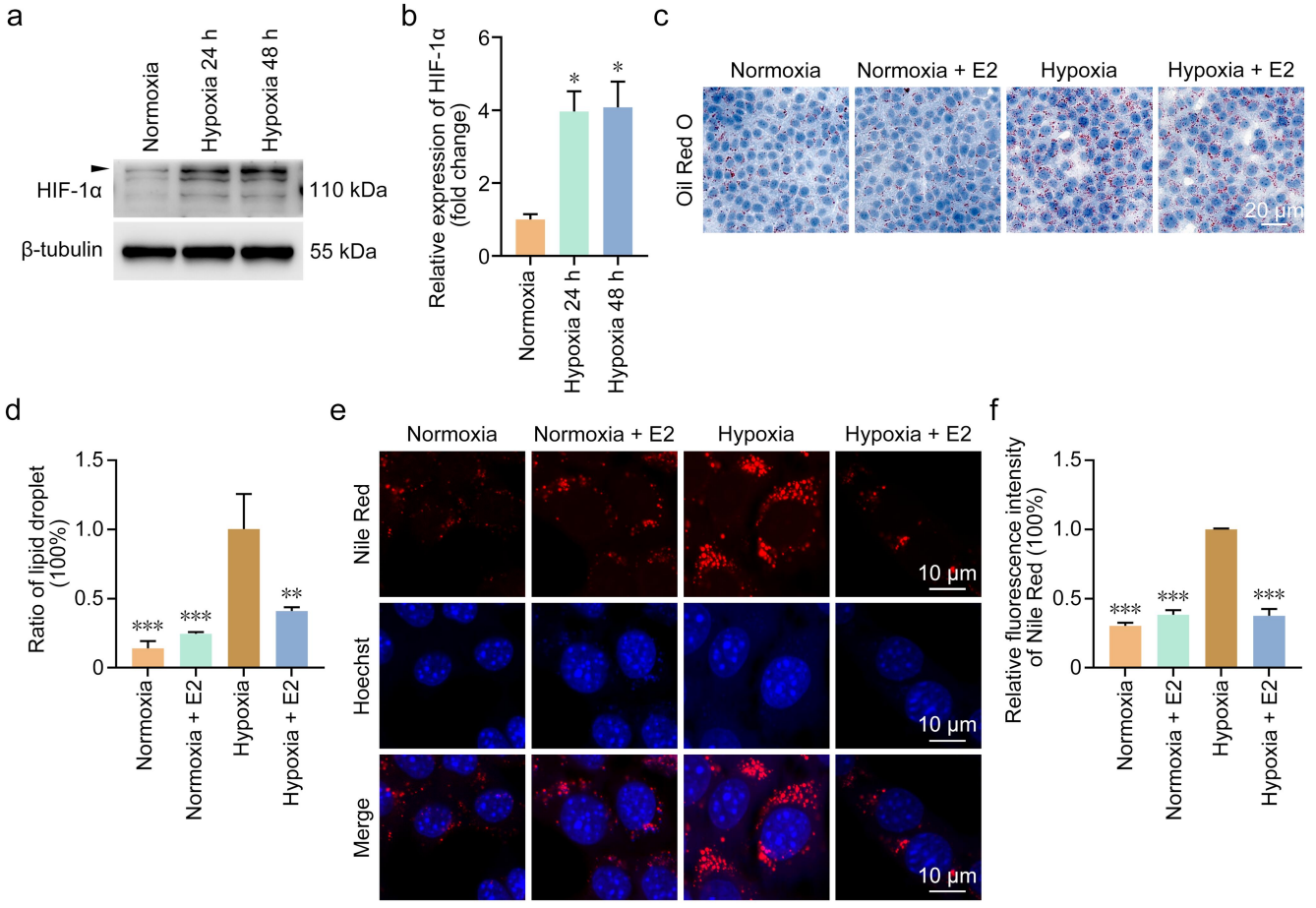


Fig. 2. Hypoxia increased HIF-1α expression in Huh-7 cells, whereas E2 attenuated hypoxia-induced lipid accumulation in AML12 cells. (a, b) Huh-7 cells were subjected to normoxia (21% O_2), hypoxia (1% O_2) for 24 h, or hypoxia (1% O_2) for 48 h, without E2 treatment. Western blotting was performed to detect the protein level of HIF-1α; β-tubulin served as the loading control. Arrowheads indicate the target protein bands. Biological replicates, $n = 3$; three technical replicate wells for each condition and one western blotting run per biological replicate. One-way ANOVA was performed, followed by Tukey's multiple-comparisons test. (c, d) AML12 cells were assigned to four experimental groups: Normoxia (21% O_2), Normoxia + E2, Hypoxia (1% O_2), Hypoxia + E2. Cells were first incubated under normoxia (21% O_2) or hypoxia (1% O_2) for 24 h, then E2 (10 nM) was administered, and cells were further cultured for another 24 h under the identical oxygen condition, with a total incubation time of 48 h. Lipid droplets were evaluated by Oil Red O staining. The average lipid droplet area per cell was analyzed using ImageJ. Images were acquired using a 20× objective. Scale bar = 20 μm. Three biological replicates per group were performed, with two technical replicate wells per biological replicate. Three random microscopic fields were captured per technical well. Lipid droplet area was normalized to the total cell number within each field. Approximately 150 cells were analyzed per group. Statistical analysis was performed using one-way ANOVA with Tukey's multiple-comparisons test. (e, f) AML12 hepatocytes were subjected to the same grouping, E2 treatment schedule, oxygen concentration, and total incubation time as in panels c, d. Intracellular lipids were visualized by Nile Red fluorescence staining, and nuclei were counterstained with Hoechst 33258. Cellular fluorescence intensity was analyzed using ImageJ software. Fluorescence images were acquired with a 63× objective lens. Scale bar = 10 μm. Biological replicates, $n = 3$. Five random fields were imaged per group in each independent biological experiment. One or two cells were analyzed in each field, yielding a total of 5–10 quantified cells per group. One-way ANOVA was performed, followed by Tukey's multiple-comparisons test. *$P < 0.05$, **$P < 0.01$, ***$P < 0.001$. For panels a, b, asterisks indicate comparison versus the Normoxia group; for panels c–f, asterisks indicate comparison versus the Hypoxia group. Data are presented as the mean ± SD. ANOVA, analysis of variance; E2, 17β-estradiol; HIF-1α, hypoxia-inducible factor 1α; SD, standard deviation.

Using the Hypoxia group as the reference, the Normoxia group showed significantly higher levels of p-Parkin (S65) and total Parkin protein (both $P < 0.001$), suggesting that hypoxia decreased the abundance of total Parkin and Ser65-phosphorylated Parkin. Compared with the Hypoxia group, the Hypoxia + E2 group showed a significant increase in p-Parkin (S65) ($P < 0.001$), accompanied by a significant increase in total Parkin protein ($P < 0.05$). Further analysis of the p-Parkin (S65)/Parkin ratio showed that it was significantly lower in the Normoxia group than in the Hypoxia group ($P < 0.01$), suggesting that hypoxia enhanced Parkin phosphorylation at Ser65. Compared with the Hypoxia group, the ratio was further increased in the Hypoxia + E2 group ($P < 0.05$). These results suggest that E2 treatment increased Parkin phosphorylation at Ser65 under hypoxia. Notably, hypoxia

 DOI: 10.14218/JTG.2026.00029 | 2026

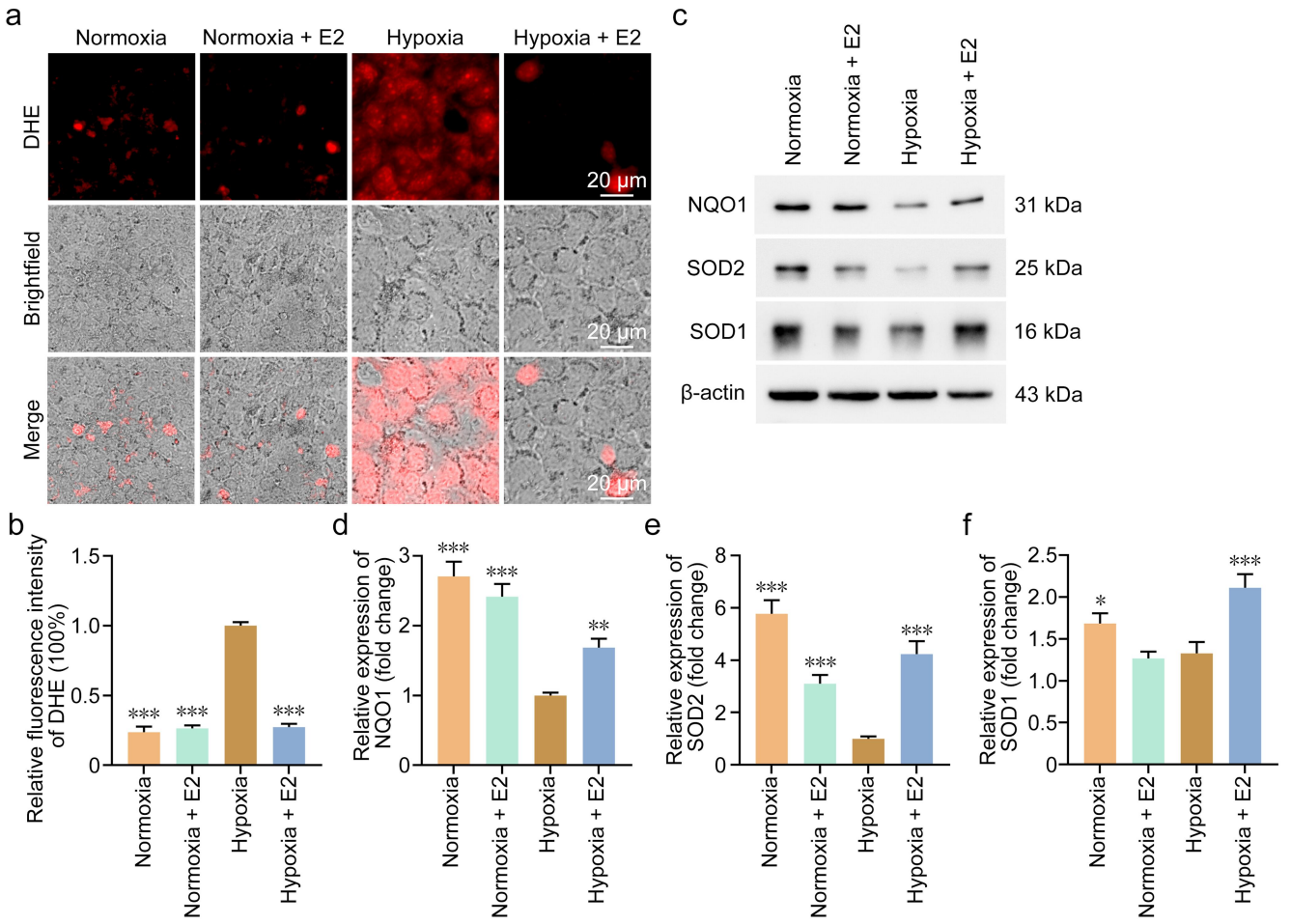


Fig. 3. E2 attenuated DHE-detectable fluorescent signals and increased antioxidant protein expression under hypoxia. (a, b) AML12 cells were used. Four experimental groups were established: Normoxia (21% O_2), Normoxia + E2, Hypoxia (1% O_2), Hypoxia + E2. Cells were first incubated under normoxia or hypoxia for 24 h, followed by E2 treatment (10 nM) for another 24 h and maintained under the same oxygen condition. The endpoint was evaluation of DHE fluorescence. Images were acquired with a 20× objective lens; scale bar = 20 μm. The relative DHE fluorescence intensity was quantified using ImageJ. Three biological replicates per group were performed, with two technical replicate wells per biological replicate, and a total of 50–100 cells were analyzed per group. One-way ANOVA was performed, followed by Tukey's multiple-comparisons test. (c–f) Huh-7 cells were used. The grouping, E2 treatment schedule, oxygen exposure conditions, and total incubation duration were the same as those described in panels a, b. The endpoint was the detection of antioxidant proteins NQO1, SOD2, and SOD1 by western blotting. β-actin was used as the internal loading control. The relative protein expression was determined by the densitometric value ratio of target protein to the corresponding internal reference. Biological replicates, n = 3. One-way ANOVA was performed, followed by Tukey's multiple-comparisons test. *P < 0.05, **P < 0.01, ***P < 0.001. All statistical comparisons were performed versus the Hypoxia group. Data are presented as the mean ± SD. ANOVA, analysis of variance; DHE, dihydroethidium; E2, 17β-estradiol; NQO1, NAD(P)H:quinone oxidoreductase 1; SD, standard deviation; SOD1, superoxide dismutase 1; SOD2, superoxide dismutase 2.

upregulated the p-Parkin/Parkin ratio, despite a decrease in total Parkin and p-Parkin levels. Under hypoxia, E2 upregulated the levels of both total Parkin and p-Parkin (Ser65), accompanied by a further increase in the p-Parkin/Parkin ratio.

We further examined the mitophagy-related proteins SQSTM1 and LC3-II (Fig. 6e–g). Under normoxia, E2 treatment slightly reduced SQSTM1 and LC3-II protein abundance, suggesting that E2 had limited effects under normoxia. Compared with the Normoxia group, hypoxia alone significantly decreased both SQSTM1 and LC3-II levels (P < 0.001). Compared with the Hypoxia group, the Hypoxia + E2 group showed a further reduction in SQSTM1 (P < 0.01) and a significant increase in LC3-II (P < 0.001). Collectively, E2 treatment further downregulated SQSTM1 and upregulated LC3-II protein levels under hypoxia.

PRKN silencing attenuated the E2-associated enhancement of mitochondrial–lysosomal colocalization under hypoxia

To verify the efficiency of *PRKN* knockdown, Parkin expression in Huh-7 cells stably transduced with sh*PRKN* or shNC was examined. Western blot analysis showed that Parkin protein abundance was reduced by 58.0% in sh*PRKN* cells compared with

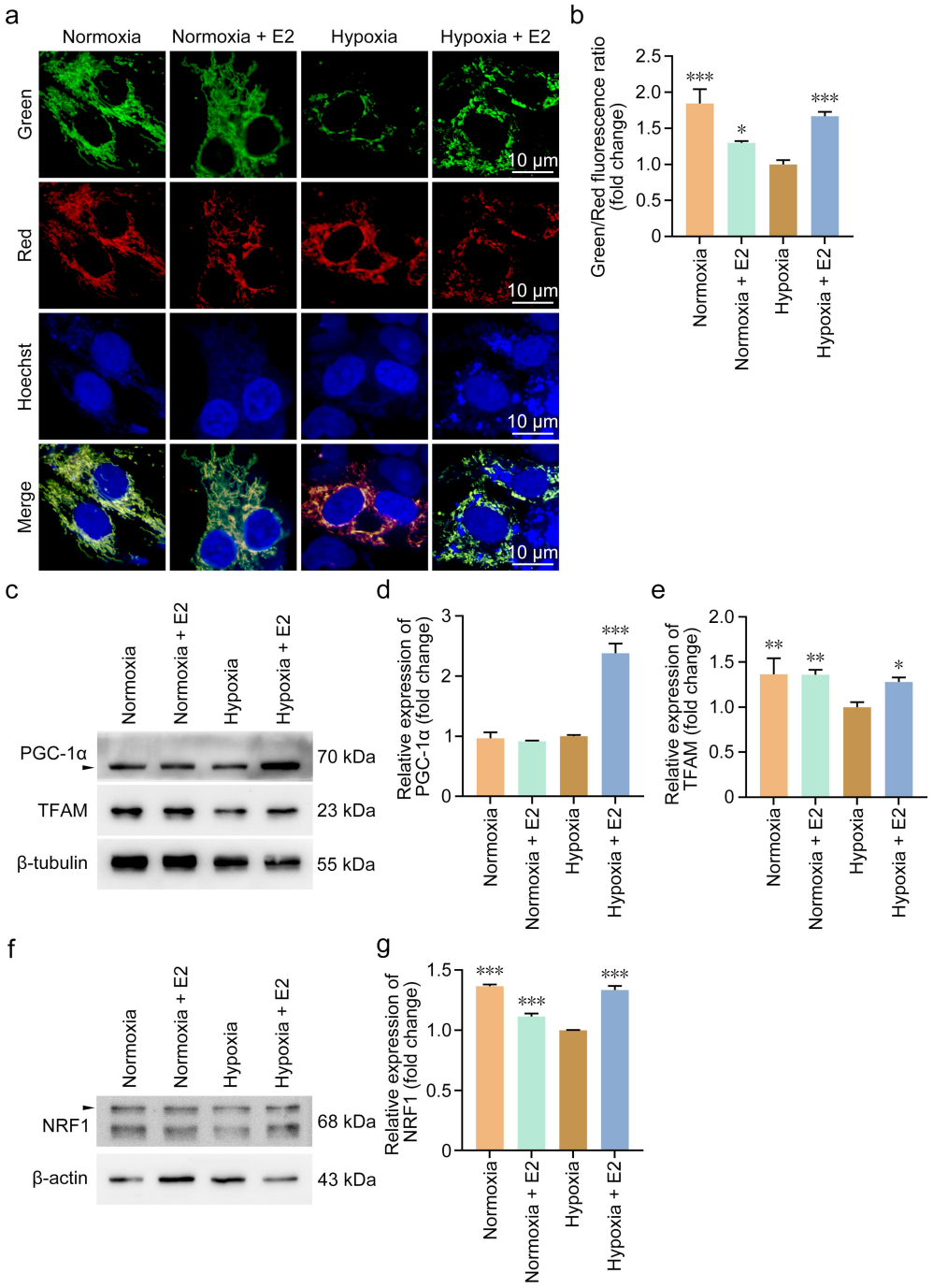


Fig. 4. E2 was associated with changes in mitochondrial protein turnover-related signals and mitochondrial biogenesis-related markers under hypoxia. (a, b) Huh-7 cells were used. Four experimental groups were established: Normoxia (21% O_2), Normoxia + E2, Hypoxia (1% O_2), Hypoxia + E2. Cells were first incubated under normoxia or hypoxia for 24 h, followed by E2 treatment (10 nM) for another 24 h and maintained under the same oxygen condition. The endpoint was evaluation of fluorescence signals associated with mitochondrial protein turnover. Images were acquired with a 63× objective lens; scale bar = 10 μm. Biological replicates, n = 3. In each independent biological experiment, five random microscopic fields were captured per group, and approximately one or two cells were analyzed per field; a total of 5–10 cells were quantified for each group per biological replicate. The green/red fluorescence ratio was calculated using ImageJ software. One-way ANOVA was performed, followed by Tukey's multiple-comparisons test. (c–g) Huh-7 cells were used. The grouping, E2 treatment schedule, oxygen exposure conditions, and total incubation duration were the same as those described in panels a, b. The endpoint was detection of mitochondrial biogenesis-associated proteins, including PGC-1α (c, d), TFAM (c, e), and NRF1 (f, g), by western

 DOI: 10.14218/JTG.2026.00029 | 2026

blotting. β-tubulin or β-actin was used as the loading control. Relative protein expression was determined by the densitometric value ratio of target protein to the corresponding internal reference. Arrowheads indicate the target protein bands. Biological replicates, n = 3. One-way ANOVA was performed, followed by Tukey's multiple-comparisons test. Data are presented as the mean ± SD. *P < 0.05, **P < 0.01, ***P < 0.001. All statistical comparisons were performed versus the Hypoxia group. ANOVA, analysis of variance; E2, 17β-estradiol; NRF1, nuclear respiratory factor 1; PGC-1α, peroxisome proliferator-activated receptor γ coactivator 1α; SD, standard deviation; TFAM, mitochondrial transcription factor A.

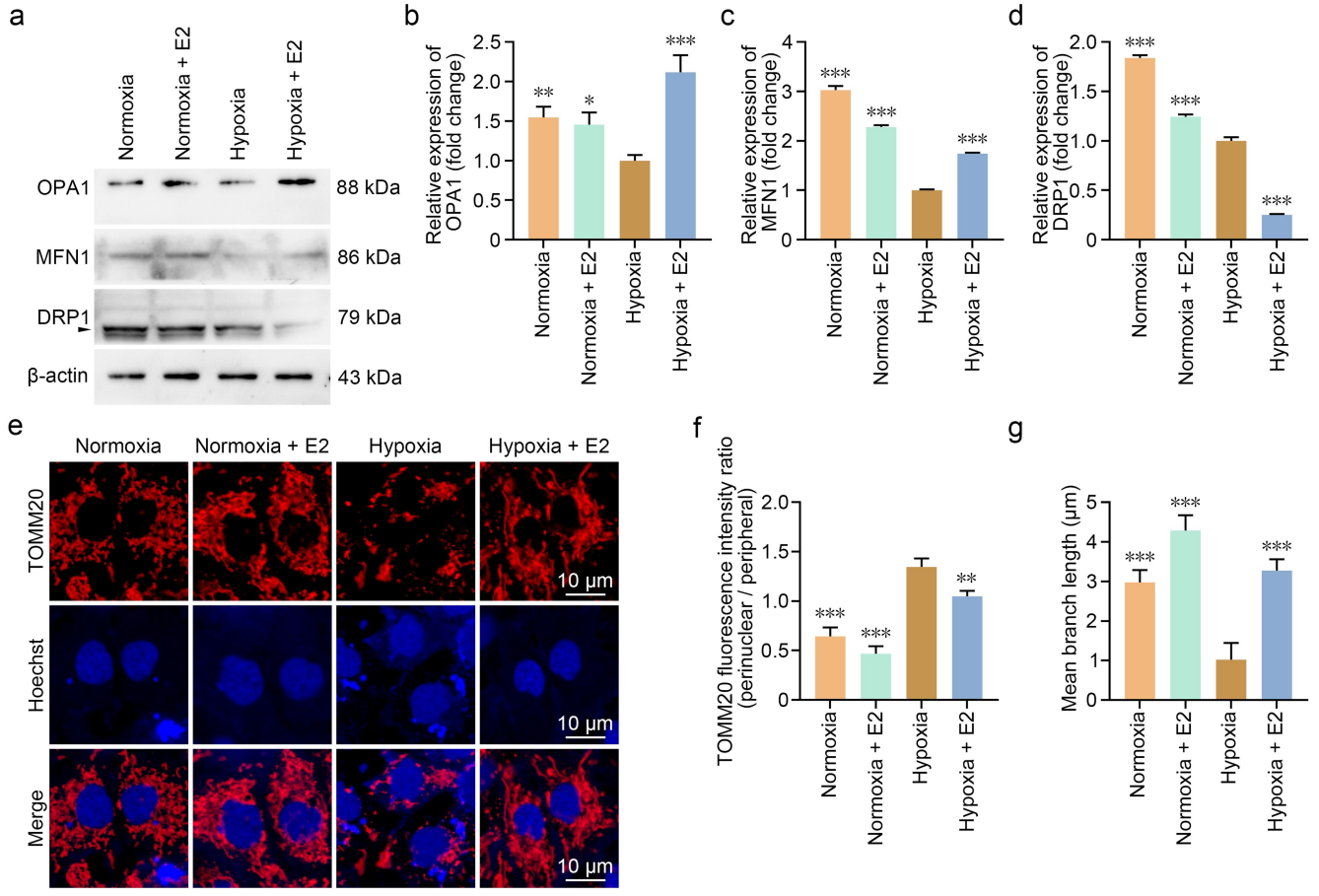


Fig. 5. E2 was associated with improved mitochondrial network morphology and changes in mitochondrial dynamics-related proteins under hypoxia. (a–d) Huh-7 cells were used. Four experimental groups were established: Normoxia (21% O_2), Normoxia + E2, Hypoxia (1% O_2), Hypoxia + E2. Cells were first incubated under normoxia or hypoxia for 24 h, followed by E2 treatment (10 nM) for another 24 h and maintained under the same oxygen condition. The endpoint was detection of mitochondrial fusion–fission-related proteins, including OPA1, MFN1, and DRP1, by western blotting. β-actin was used as the internal loading control. Relative protein expression was determined by the densitometric value ratio of target protein to the corresponding internal reference. Arrowheads indicate the target protein bands. Biological replicates, n = 3. One-way ANOVA was performed, followed by Tukey's multiple-comparisons test. (e–g) Huh-7 cells were used. The grouping, E2 treatment schedule, oxygen exposure conditions, and total incubation duration were the same as those described in panels a–d. The endpoint was TOMM20 immunofluorescence staining. Images were acquired with a 63× objective lens; scale bar = 10 μm. Biological replicates, n = 3. In each independent biological experiment, five random microscopic fields were captured per group, and approximately one or two cells were analyzed per field. A total of 5–10 cells were quantified for each group per biological replicate. ImageJ was applied to quantify the TOMM20 fluorescence intensity ratio (perinuclear/peripheral) and the mean mitochondrial branch length. Data are presented as the mean ± SD. One-way ANOVA was performed, followed by Tukey's multiple-comparisons test. *P < 0.05, **P < 0.01, ***P < 0.001. All statistical comparisons were performed versus the Hypoxia group. ANOVA, analysis of variance; DRP1, dynamin-related protein 1; E2, 17β-estradiol; MFN1, mitofusin 1; OPA1, optic atrophy 1; SD, standard deviation; TOMM20, translocase of outer mitochondrial membrane 20.

shNC cells (0.42 ± 0.12 *vs.* 1.00 ± 0.12, n = 3 independent biological replicates, P < 0.01), confirming successful *PRKN* knockdown (Fig. 7a, b).

Line-scan analysis was performed to examine changes in mitochondrial and lysosomal fluorescence signals under different oxygen conditions and E2 treatments. In the Normoxia group, the

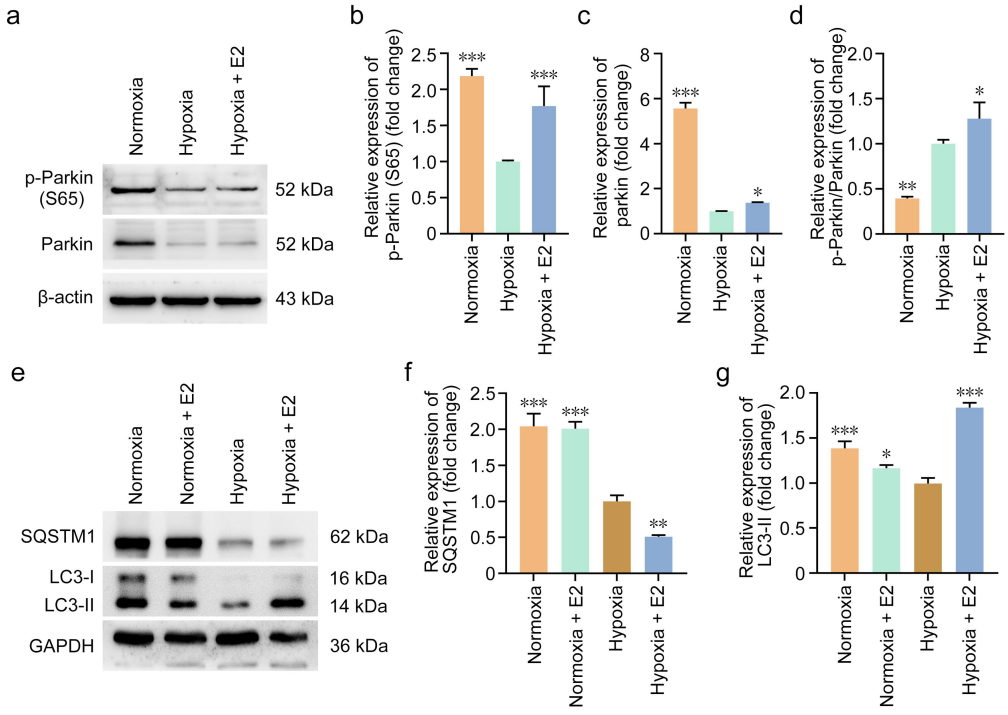


Fig. 6. E2 was associated with altered Parkin phosphorylation and expression of mitophagy-related proteins under hypoxia. (a–d) Huh-7 cells were used. Three experimental groups were established: Normoxia (21% O_2), Hypoxia (1% O_2), Hypoxia + E2. Cells were first incubated under normoxia or hypoxia for 24 h, followed by E2 treatment (10 nM) for another 24 h, and maintained at the same oxygen condition. The endpoint was to detect Parkin expression and phosphorylation at Ser65 by western blotting. β-actin was used as the internal loading control. Relative protein expression was determined by the densitometric value ratio of target protein to the corresponding internal reference. For quantification of the p-Parkin (S65)/Parkin ratio, p-Parkin and total Parkin were first individually normalized to β-actin. The normalized p-Parkin value was then divided by the normalized total Parkin value, and the resulting ratio was normalized to the Hypoxia group (set as 1) for plotting. Biological replicates, n = 3. One-way ANOVA was performed, followed by Tukey's multiple-comparisons test. (e–g) Huh-7 cells were used. Four experimental groups were established: Normoxia (21% O_2), Normoxia + E2, Hypoxia (1% O_2), Hypoxia + E2. Cells were first incubated under normoxia or hypoxia for 24 h, followed by E2 treatment for another 24 h and maintained under the same oxygen condition. The endpoint was the detection of mitophagy markers, including SQSTM1 and LC3, by western blotting. GAPDH was used as the internal loading control. Relative protein expression was determined by the densitometric value ratio of target protein to the corresponding internal reference. Biological replicates, n = 3. Data are presented as the mean ± SD. One-way ANOVA was performed, followed by Tukey's multiple-comparisons test. *P < 0.05, **P < 0.01, ***P < 0.001. All statistical comparisons were performed versus the Hypoxia group. ANOVA, analysis of variance; E2, 17β-estradiol; GAPDH, glyceraldehyde-3-phosphate dehydrogenase; LC3, microtubule-associated protein light chain 3; p-Parkin (S65), Ser65-phosphorylated Parkin; SD, standard deviation; SQSTM1, sequestosome 1.

green LAMP1-GFP and red TOMM20 fluorescence curves showed some overlap (Fig. 7c, d). However, no obvious synchronous changes or downward troughs were observed in the red TOMM20 curve, suggesting a certain degree of mitochondrial–lysosomal proximity or colocalization under normoxia. In contrast, relatively few colocalization-associated signal changes were observed. Compared with the Normoxia group, the Normoxia + E2 group also showed some overlap between the red and green fluorescence curves, without an obvious increase in synchronous changes or a characteristic decrease in TOMM20 fluorescence, suggesting that E2 did not markedly increase mitochondrial–lysosomal colocalization or related fluorescence signals under normoxia (Fig. 7e). In contrast, the Hypoxia group showed a relatively shallow local decrease in red TOMM20 fluorescence, accompanied by changes in the LAMP1-GFP signal, suggesting limited mitochondrial–lysosomal colocalization and associated fluorescence signal changes under hypoxia (Fig. 7f). Compared with the Hypoxia group, both the red TOMM20 fluorescence and green LAMP1-GFP signals in the Hypoxia + E2 group fluctuated at comparable intensity levels (Fig. 7g). The two signals partially overlapped, suggesting that E2 enhanced mitochondrial–lysosomal colocalization and associated fluorescence signal changes under hypoxia.

As shown in Figure 7h, i, line-scan analysis in the sh*PRKN* group showed that the red TOMM20 fluorescence signal first decreased, then increased. However, its overlap with the green LAMP1-GFP fluorescence curve was relatively limited, suggesting that *PRKN* silencing reduced mitochondrial–lysosomal colocalization-related signals. Compared with the sh*PRKN* group, the sh*PRKN* + E2 group still showed no obvious synchronous changes between the red and green fluorescence signals, and the TOMM20 curve did not decrease more than in the sh*PRKN* group (Fig. 7j). These findings suggest that E2 failed to markedly enhance mitochondrial–lysosomal colocalization or related fluor-

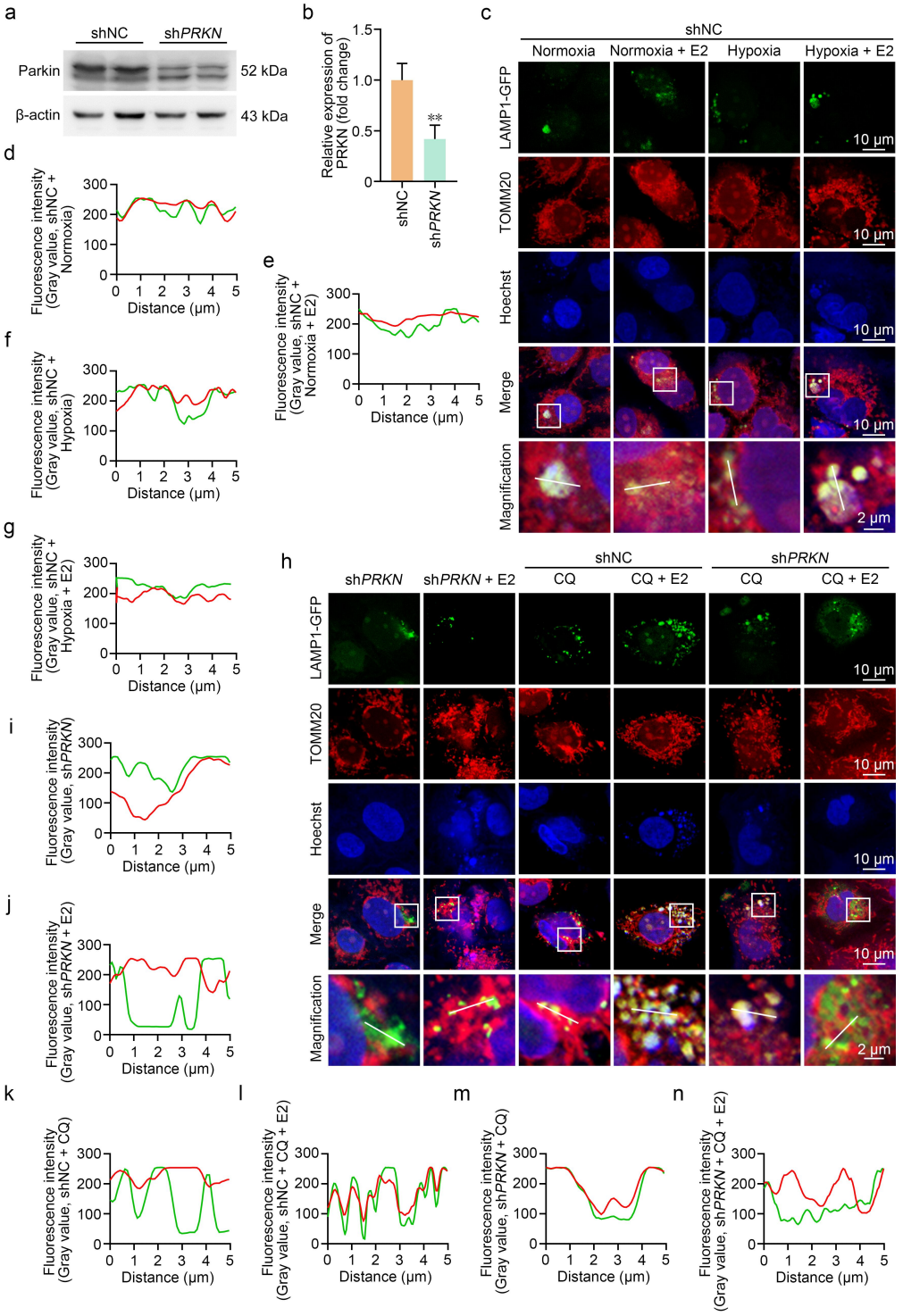


Fig. 7. *PRKN* silencing attenuated the E2-associated enhancement of mitochondrial–lysosomal colocalization under hypoxia. (a, b) The efficiency of *PRKN* knockdown in Huh-7 cells was assessed by western blotting and quantified by densitometry. β-actin was used as the internal loading control. Parkin protein abundance was normalized to β-actin and expressed relative to the shNC group (n = 3). Statistical analysis was performed using an unpaired two-tailed Student's t-test. Data in panel b are presented as the mean ± SD. $^{**}P < 0.01$ versus the shNC group. (c–g) Huh-7-shNC cells were used. Four experimental groups were established: Normoxia (21% O_2), Normoxia + E2, Hypoxia (1% O_2), Hypoxia + E2. Cells were first transfected with pEGFP-N1-

LAMP1, a plasmid expressing a fusion protein in which enhanced green fluorescent protein is fused to the C-terminus of LAMP1 (LAMP1-GFP). Afterward, cells were incubated under normoxia or hypoxia for 24 h, followed by E2 treatment (10 nM) for another 24 h, under the same oxygen condition. Exogenously expressed LAMP1-GFP (lysosomes, green) and immunofluorescence-stained endogenous TOMM20 (mitochondria, red) were imaged to examine their spatial relationship. Nuclei were counterstained with Hoechst (blue). Images were acquired with a 63× objective lens; scale bar = 10 μm (magnified inset: 2 μm). Images are representative of three independent biological experiments. In each experiment, five random microscopic fields were captured per group, and approximately one or two cells were examined per field, yielding 5–10 cells per group per experiment. Line-scan analysis of LAMP1-GFP and TOMM20 fluorescence intensity was performed using ImageJ to illustrate the spatial relationship between the two fluorescence signals along selected lines. No group-level colocalization quantification or inferential statistical analysis was performed for these panels. (h–n) Huh-7 cells were used. All treatments were performed under hypoxia (1% O_2). Six experimental groups were established. Two groups (CQ and CQ + E2) were generated using shNC Huh-7 control cells, while the remaining four groups were based on Huh-7-sh*PRKN* stable knockdown cells: sh*PRKN*, sh*PRKN* + E2, sh*PRKN* + CQ, sh*PRKN* + E2 + CQ. Stable Huh-7-shNC and Huh-7-sh*PRKN* cells were transfected with pEGFP-N1-LAMP1. Subsequently, cells were incubated under hypoxia for 24 h. Then E2 (10 nM) was added, and cells were incubated for an additional 24 h under hypoxia. CQ (10 μM) was added during the final 6 h of the second 24 h incubation period. Hypoxia was maintained throughout the 48 h treatment period. LAMP1-GFP fluorescence (lysosomes, green) and immunofluorescence-stained endogenous TOMM20 (mitochondria, red) were imaged to examine their spatial relationship. Nuclei were counterstained with Hoechst (blue). Images were acquired with a 63× objective lens; scale bar = 10 μm (magnified inset: 2 μm). Images are representative of three independent biological experiments. In each experiment, five random microscopic fields were captured per group, and approximately one or two cells were examined per field, yielding 5–10 cells per group per experiment. Line-scan analysis of LAMP1-GFP and TOMM20 fluorescence intensity was performed using ImageJ to illustrate the spatial relationship between the two fluorescence signals along selected lines. No group-level colocalization quantification or inferential statistical analysis was performed for these panels. ANOVA, analysis of variance; CQ, chloroquine; E2, 17β-estradiol; GFP, green fluorescent protein; LAMP1, lysosome-associated membrane protein 1; *PRKN*, parkin RBR E3 ubiquitin protein ligase gene; SD, standard deviation; shNC, non-targeting control short hairpin RNA; sh*PRKN*, short hairpin RNA targeting *PRKN*; TOMM20, translocase of outer mitochondrial membrane 20.

escence signal changes in the context of *PRKN* silencing. In the shNC + CQ group, the red TOMM20 and green LAMP1-GFP fluorescence curves showed marked synchronous changes with some overlap. However, no obvious sustained decrease in TOMM20 fluorescence was observed (Fig. 7k). Compared with the shNC + CQ group, the shNC + CQ + E2 group showed further increases in the synchrony and overlap of the red and green fluorescence curves, suggesting that E2 further increased the accumulation of mitochondrial–lysosomal colocalization-related signals under hypoxia in the presence of CQ (Fig. 7l). Compared with the sh*PRKN* group, the sh*PRKN* + CQ group showed more pronounced synchronous changes and greater overlap between the red TOMM20 and green LAMP1-GFP fluorescence curves, with both curves displaying a similar W-shaped pattern (Fig. 7m). These findings suggest that, even with *PRKN* silencing, CQ treatment was associated with detectable accumulation of mitochondrial–lysosomal colocalization-related signals. In the sh*PRKN* + CQ + E2 group, the red TOMM20 and green LAMP1-GFP fluorescence curves did not show the pronounced synchronous overlap observed in the sh*PRKN* + CQ group. Instead, they showed relatively interleaved fluctuations, accompanied by a clear downward trough in the TOMM20 curve (Fig. 7n). Compared with the sh*PRKN* + CQ group, the sh*PRKN* + CQ + E2 group showed no further increase in the synchrony or overlap of the red and green fluorescence curves, suggesting that E2 did not further promote mitochondrial–lysosomal colocalization in the context of *PRKN* silencing. Compared with the shNC + CQ + E2 group, the sh*PRKN* + CQ + E2 group showed less synchronous enhancement of the red and green fluorescence signals, suggesting that *PRKN* silencing attenuated the E2-associated changes in mitochondrial–lysosomal colocalization-related signals.

PRKN silencing altered the effects of E2 on hypoxia-induced lipid accumulation and DHE fluorescent signals in Huh-7 cells

As shown in Figure 1a–c, cells in the shNC group under normoxia showed relatively weak Nile Red fluorescence, indicating relatively low lipid accumulation. However, the shNC + Normoxia + E2 group showed a slight increase in fluorescence compared with the shNC + Normoxia group. Hypoxia markedly increased Nile Red fluorescence compared with the shNC + Normoxia group, indicating that hypoxia promoted intracellular lipid accumulation ($P < 0.001$). Compared with the shNC + Hypoxia group, Nile Red fluorescence was significantly reduced in the shNC + Hypoxia + E2 group ($P < 0.001$), suggesting that E2 alleviated hypoxia-induced lipid accumulation. Compared with the shNC + Hypoxia group, Nile Red fluorescence increased further in the sh*PRKN* + Hypoxia group ($P < 0.001$), indicating that hypoxia-induced lipid accumulation was more pronounced after *PRKN* silencing. As shown in Figure 1c, two-way ANOVA revealed a significant interaction between *PRKN* status and E2 treatment [$F(1, 8) = 63.61$, $P < 0.001$, partial $\eta^2 = 0.89$], indicating that *PRKN* status significantly modified the effect of E2 on Nile Red fluorescence. Significant main effects of *PRKN* status [$F(1, 8) = 715.3$, $P < 0.001$, partial $\eta^2 = 0.99$] and E2 treatment [$F(1, 8) = 1110$, $P < 0.001$, partial $\eta^2 = 0.99$] were also detected. Under hypoxia, Nile Red fluorescence remained significantly higher in the sh*PRKN* + E2 group than in the shNC + E2 group ($P < 0.001$). Specifically, E2 treatment reduced Nile Red fluorescence from 1.00 to 0.43 in shNC cells and from 1.78 to 0.85 in sh*PRKN* cells, corresponding to relative reductions of 57.0% and 52.2%, respectively. Despite the E2-associated reduction in both groups, Nile Red fluorescence in the sh*PRKN* + E2 group remained approximately 1.98-fold that in the shNC + E2 group. Together with the significant *PRKN* status × E2 treatment interaction, these findings indicate that *PRKN* status significantly modified the effect of E2 on lipid accumulation and that *PRKN* knockdown was associated with a higher residual level of lipid accumulation after E2 treatment.

As shown in Figure 1d–f, hypoxia markedly increased DHE fluorescence ($P < 0.001$), indicating higher DHE-detectable fluorescence under hypoxia. Compared with the Hypoxia group,

 DOI: 10.14218/JTG.2026.00029 | 2026

DHE fluorescence was significantly reduced in the Hypoxia + E2 group ($P < 0.001$), suggesting that E2 reduced hypoxia-induced oxidative signals. Further analysis in the sh*PRKN* background showed that DHE fluorescence increased markedly under hypoxia ($P < 0.001$) and was overall higher than in the shNC Hypoxia group. Under hypoxia, E2 treatment significantly reduced DHE fluorescence in sh*PRKN* cells ($P < 0.001$). As shown in Figure 1f, two-way ANOVA also revealed a significant interaction between *PRKN* status and E2 treatment [$F(1, 8) = 40.51$, $P = 0.0002$, partial $\eta^2 = 0.84$], indicating that *PRKN* status significantly modified the effect of E2 on DHE fluorescence. Significant main effects of *PRKN* status [$F(1, 8) = 993.7$, $P < 0.001$, partial $\eta^2 = 0.99$] and E2 treatment [$F(1, 8) = 352.3$, $P < 0.001$, partial $\eta^2 = 0.98$] were also detected. Specifically, E2 treatment decreased DHE fluorescence from 1.00 to 0.82 in shNC cells and from 1.55 to 1.18 in sh*PRKN* cells. The corresponding relative reductions were 18.0% and 23.9%, respectively, indicating that the E2-associated decrease was not attenuated by *PRKN* knockdown on a relative basis. Nevertheless, DHE fluorescence in the sh*PRKN* + E2 group remained significantly higher than that in the shNC + E2 group ($P < 0.001$), at approximately 1.44-fold the level in the shNC + E2 group. Thus, the significant *PRKN* status × E2 treatment interaction indicates that *PRKN* status modified the overall DHE fluorescence response to E2, rather than reducing the magnitude of the E2-associated decrease itself.

Discussion

This study shows that E2 alleviates hypoxia-induced lipid accumulation and DHE fluorescent signals in Huh-7 and AML12 cells and is associated with changes in MQC-related processes. However, this study provides evidence only that E2 regulates hypoxia-associated lipid accumulation and MQC-related changes in cultured hepatocytes. Whether these effects apply to chronic hypoxia at high altitude requires validation in animal models and clinical trials.

Previous studies suggested that E2 can alleviate lipid metabolism-related disorders, exert antioxidant effects, and maintain mitochondrial function.[22] However, it remains unclear whether E2 ameliorates hypoxia-induced hepatic lipid accumulation. Here, using hypoxic Huh-7 and AML12 hepatocytes, we found that E2 significantly alleviated hypoxia-triggered lipid deposition. Consistent with our findings, previous *in vivo* studies showed that E2 reduced liver lipid accumulation in mice with MASLD, although those studies did not involve hypoxic exposure.[23] Although hypoxia-induced hepatocyte lipid accumulation is closely related to HIF-2α, no study has reported E2's regulatory role in this pathological process.[24] Our observations provide preliminary evidence of this regulatory role. E2 can attenuate oxidative stress in cardiovascular and neurological diseases.[25,26] In AML12 and HepG2 cells, E2 may decrease ROS production by enhancing thioredoxin 2 activity and relieving lipid peroxidation-induced oxidative injury.[27] Consistent with these findings, our results showed that E2 attenuated hypoxia-induced DHE fluorescent signals in hepatocytes. E2's protective effect on mitochondrial function has been documented.[28] The context-dependent nature of antioxidant regulation should also be considered, as Keap1–NRF2–ARE signaling may exert divergent effects on lipid accumulation and oxidative injury in steatotic liver disease.[29] It has been demonstrated that E2 maintains mitochondrial membrane potential stability in cardiomyocytes and neurons, thereby reducing mitochondrial damage.[30,31] Similarly, this study found that E2 was associated with reduced hypoxia-induced oxidative signals and improvements in MQC-related abnormalities in hypoxic hepatocytes, suggesting a protective effect on these cells.

To further investigate whether *PRKN*-related processes contribute to E2's protective effects, we silenced *PRKN* and examined both mitochondrial–lysosomal colocalization and downstream cellular phenotypes. Consistent with these findings, two-way ANOVA revealed significant *PRKN* status × E2 treatment interactions for both Nile Red and DHE fluorescence under hypoxia. For lipid accumulation, *PRKN* knockdown significantly altered the responses to E2, with Nile Red fluorescence remaining substantially higher in sh*PRKN* + E2 cells than in shNC + E2 cells. For DHE fluorescence, E2 retained a significant reducing effect after *PRKN* knockdown, and the relative reduction was not diminished in sh*PRKN* cells. Therefore, the significant *PRKN* status × E2 treatment interaction should be interpreted as a modification of the overall response pattern rather than as attenuation of the E2-associated decrease. Notably, DHE fluorescence remained markedly higher in sh*PRKN* + E2 cells than in shNC + E2 cells, indicating a persistently higher oxidative signal in *PRKN*-knockdown cells despite E2 treatment. These findings indicate that *PRKN* contributes to, but is not solely responsible for, the protective effects of E2 on lipid accumulation and oxidative signals under hypoxia. Together with the mitochondrial–lysosomal colocalization data, they support the involvement of *PRKN*-related processes in the mitochondrial response to E2 while also suggesting the presence of additional *PRKN*-independent pathways. This immunofluorescence-based assay primarily monitors mitochondrial delivery to lysosomes. Therefore, these observations should not be considered equivalent to direct measurement of complete mitophagic degradation dynamics.

In addition to *PRKN*-dependent mitochondrial autophagy, hypoxia also influenced MQC, including mitochondrial biogenesis and dynamics. Pharmacological modulation of mitochondrial dysfunction, including regulation of MQC, has attracted increasing interest as a potential strategy for restoring mitochondrial homeostasis.[32] MitoTimer analysis revealed shifted green-to-red fluorescence ratios, indicating altered turnover of mitochondrial reporter proteins, although this assay cannot directly quantify mitochondrial biogenesis. Hypoxia induced abnormal expression of biogenesis-related markers including TFAM, PGC-1α, and NRF1, and E2 partially rescued these alterations. These observations suggest that E2 may alleviate hypoxia-induced disturbances in biogenesis-associated markers, yet MitoTimer data alone cannot prove enhanced mitochondrial biogenesis. At the level of mitochondrial dynamics, E2 treatment increased OPA1 and MFN1 while decreasing DRP1. Consistent with these protein changes, TOMM20-based imaging showed remodeled mitochondrial networks after E2 intervention. Notably, neither the steady-state levels of these dynamics-related proteins nor TOMM20 morphological metrics directly measure mitochondrial fission–fusion rates. Accordingly, these results support only an association between E2 and mitochondrial network remodeling, rather than providing direct evidence of altered fission–fusion kinetics.

This study has several inherent limitations. First, all experiments were performed in Huh-7 and AML12 cell models, which do not recapitulate the complex *in vivo* hepatic microenvironment or the chronic hypoxic characteristics of high altitude. Second, this study lacks *in vivo* animal validation and pharmacokinetic evaluation of E2, so the protective efficacy and biosafety of E2 under chronic hypoxia remain unclear. Third, although *PRKN* silencing and mitochondrial–lysosomal colocalization analyses support the involvement of *PRKN*-related processes, the current assays cannot precisely confirm the dynamics of complete mitophagic degradation. Fourth, changes in mitochondrial morphological parameters, dynamics, protein expression, and MitoTimer signals reflect only mitochondrial network remodeling and protein turnover, which are insufficient to quantify mitochondrial fission–fusion activity and biogenesis directly. In addition, we used a conventional phenol-red-containing medium and non-charcoal-stripped FBS, and we cannot completely exclude potential background estrogenic activity from the culture system. Fifth, this study did not identify the specific estrogen receptor subtype mediating E2-induced protection, leaving the upstream molecular mechanism of E2 regulation uncharacterized. Estrogen receptor α-mediated reporter assays combined with receptor antagonism provide an established approach for evaluating estrogen receptor α-dependent estrogenic responses and may help clarify the upstream receptor mechanism in future studies.[33]

Conclusions

E2 attenuates hypoxia-induced lipid accumulation and DHE fluorescent signals in hepatocytes *in vitro* and is associated with improvements in multiple MQC-related responses. *PRKN* silencing alters several E2-associated protective effects, supporting the involvement of *PRKN*-related processes, although the precise receptor-dependent and mitochondrial mechanisms require further investigation.

Acknowledgements

None.

Funding

This study was supported by the National Natural Science Foundation of China (Grant No. 82270613).

Conflict of interest

The authors declare no conflicts of interest.

Author contributions

Conceptualization (XDS); methodology (YJY, JDW); investigation (JHL, NLW); formal analysis (JHL, NLW, YJY); resources (JDW, LPC, JCX, YHX); writing – original draft (JHL, NLW); writing – review and editing (YJY, JDW, LPC, JCX, YHX, YYZ, XDS); supervision (YYZ, XDS); project administration (YYZ, XDS); funding acquisition (XDS). All authors have approved the final version and publication of the manuscript.

Ethical statement

The study used only established cell lines (Huh-7 and AML12) and did not involve human participants, human specimens, or animal experiments. Therefore, ethics approval was not required.

Data sharing statement

The data supporting the findings of the study are available from the corresponding author upon reasonable request.

References

[1] Nath B, Szabo G. Hypoxia and hypoxia inducible factors: diverse roles in liver diseases. Hepatology 2012;55(2):622–633. DOI: 10.1002/hep.25497, PMID: 22120903.

[2] Siques P, Brito J, Naveas N, Pulido R, De la Cruz JJ, Mamani M, *et al*. Plasma and liver lipid profiles in rats exposed to chronic hypobaric hypoxia: changes in metabolic pathways. High Alt Med Biol 2014;15(3):388–395. DOI: 10.1089/ham.2013.1134, PMID: 25185022.

[3] Dong X, Li JM, Lu XL, Lin XY, Hong MZ, Weng S, *et al*. Global burden of adult non-alcoholic fatty liver disease (NAFLD) and non-alcoholic steatohepatitis (NASH) has been steadily increasing over the past decades and is expected to persist in the future. Transl Gastroenterol Hepatol 2024;9:33. DOI: 10.21037/tgh-23-118, PMID: 39091655.

[4] Riazi K, Azhari H, Charette JH, Underwood FE, King JA, Afshar EE, *et al*. The prevalence and incidence of NAFLD worldwide: a systematic review and meta-analysis. Lancet Gastroenterol Hepatol 2022;7(9):851–861. DOI: 10.1016/S2468-1253(22)00165-0, PMID: 35798021.

[5] Li B, Piao S, Fu Y, Fu Q, Qin P, Kong W, *et al*. Lipid metabolism-MAFLD crosstalk: mechanisms and therapy. Front Endocrinol (Lausanne) 2026;17:1785178. DOI: 10.3389/fendo.2026.1785178, PMID: 41928880.

[6] Song L, Huang Y, Liu L, Chang X, Hu L, Wang G, *et al*. Meteorin-like alleviates hepatic steatosis by regulating hepatic triglyceride secretion and fatty acid oxidation. Cell Rep 2025;44(2):115246. DOI: 10.1016/j.celrep.2025.115246, PMID: 39918960.

[7] Boone C, Lewis SC. Bridging lipid metabolism and mitochondrial genome maintenance. J Biol Chem 2024;300(8):107498. DOI: 10.1016/j.jbc.2024.107498, PMID: 38944117.

[8] Ma Q, Liu K, Chang C, Wang L, Shen Z, Li J, *et al*. Metabolic dysfunction-associated steatotic liver disease: Pathogenesis, model and treatment (Review). Int J Mol Med 2025;56(6):227. DOI: 10.3892/ijmm.2025.5668, PMID: 41104870.

[9] Radosavljevic T, Brankovic M, Samardzic J, Djuretić J, Vukicevic D, Vucevic D, *et al*. Altered Mitochondrial Function in MASLD: Key Features and Promising Therapeutic Approaches. Antioxidants (Basel) 2024;13(8):906. DOI: 10.3390/antiox13080906, PMID: 39199152.

[10] Li J, Liu W, Zhang J, Sun C. The Role of Mitochondrial Quality Control in Liver Diseases: Dawn of a Therapeutic Era. Int J Biol Sci 2025;21(4):1767–1783. DOI: 10.7150/ijbs.107777, PMID: 39990657.

[11] Li Q, Huang Y. Mitochondrial targeted strategies and their application for cancer and other diseases treatment. J Pharm Investig 2020;50:271–293. DOI: 10.1007/s40005-020-00481-0.

[12] Martin-Grau M, Monleon D. Sex dimorphism and metabolic profiles in management of metabolic-associated fatty liver disease. World J Clin Cases 2023;11(6):1236–1244. DOI: 10.12998/wjcc.v11.i6.1236, PMID: 36926130.

[13] Chen XY, Wang C, Huang YZ, Zhang LL. Nonalcoholic fatty liver disease shows significant sex dimorphism. World J Clin Cases 2022; 10(5):1457–1472. DOI: 10.12998/wjcc.v10.i5.1457, PMID: 35211584.

[14] Robeva R, Mladenović D, Vesković M, Hrnčić D, Bjekić-Macut J, Stanojlović O, *et al*. The interplay between metabolic dysregulations and non-alcoholic fatty liver disease in women after menopause. Maturitas 2021;151:22–30. DOI: 10.1016/j.maturitas.2021.06.012, PMID: 34446275.

[15] Huang X, Pan CH, Yin F, Peng J, Yang L. The Role of Estrogen in Mitochondrial Disease. Cell Mol Neurobiol 2025;45(1):68. DOI: 10.1007/s10571-025-01592-8, PMID: 40643846.

[16] Cho EJ, Choi Y, Jung SJ, Kwak HB. Role of exercise in estrogen deficiency-induced sarcopenia. J Exerc Rehabil 2022;18(1):2–9. DOI: 10.12965/jer.2244004.002, PMID: 35356136.

[17] Beikoghli Kalkhoran S, Kararigas G. Oestrogenic Regulation of Mitochondrial Dynamics. Int J Mol Sci 2022;23(3):1118. DOI: 10.3390/ijms23031118, PMID: 35163044.

[18] Sasaki Y, Ikeda Y, Uchikado Y, Akasaki Y, Sadoshima J, Ohishi M. Estrogen Plays a Crucial Role in Rab9-Dependent Mitochondrial Autophagy, Delaying Arterial Senescence. J Am Heart Assoc 2021; 10(7):e019310. DOI: 10.1161/JAHA.120.019310, PMID: 33719502.

[19] Xu L, Xu J, Shi W, Zhang S, Guo T, Zou S. Decreased protein activator of interferon induced protein kinase (PRKRA) involved in menopause-related cholesterol metabolic disorders by regulating cholesterol biosynthesis. Lipids Health Dis 2025;24(1):171. DOI: 10.1186/s12944-025-02575-w, PMID: 40349061.

[20] Zhang L, Ma Y, Liu M, Ma Y, Guo H. The effects of various estrogen doses on the proliferation and differentiation of cultured neural stem cells. Gen Physiol Biophys 2019;38(5):417–425. DOI: 10.4149/gpb_2019022, PMID: 31411572.

[21] Yang Y, Wu Y, Zou J, Wang YH, Xu MX, Huang W, *et al*. Naringenin Attenuates Non-Alcoholic Fatty Liver Disease by Enhancing Energy Expenditure and Regulating Autophagy via AMPK. Front Pharmacol 2021;12:687095. DOI: 10.3389/fphar.2021.687095, PMID: 34163366.

[22] Zhu L, Brown WC, Cai Q, Krust A, Chambon P, McGuinness OP, *et al*. Estrogen treatment after ovariectomy protects against fatty liver and may improve pathway-selective insulin resistance. Diabetes 2013;62(2):424–434. DOI: 10.2337/db11-1718, PMID: 22966069.

[23] Afonso-Alí A, Dicroce-Giacobini J, Teixido-Trujillo S, Porrini E, Pérez-Pérez JA, García-Hernández S, *et al*. Role of obesity and estrogen deficiency in non-alcoholic fatty liver disease: Insights from a mouse model. Mol Med Rep 2025;32(4):264. DOI: 10.3892/mmr.2025.13629, PMID: 40709389.

[24] Chen J, Chen J, Fu H, Li Y, Wang L, Luo S, *et al*. Hypoxia exacerbates nonalcoholic fatty liver disease via the HIF-2α/PPARα pathway. Am J Physiol Endocrinol Metab 2019;317(4):E710–E722. DOI: 10.1152/ajpendo.00052.2019, PMID: 31430204.

[25] Xiang D, Liu Y, Zhou S, Zhou E, Wang Y. Protective Effects of Estrogen on Cardiovascular Disease Mediated by Oxidative Stress. Oxid Med Cell Longev 2021;2021:5523516. DOI: 10.1155/2021/5523516, PMID: 34257804.

[26] Lu J, Xian TJ, Li CJ, Wang Y. The estrogen-brain interface in neuroinflammation: a multidimensional mechanistic insight. Front Aging Neurosci 2025;17:1671552. DOI: 10.3389/fnagi.2025.1671552, PMID: 40959795.

[27] Smiriglia A, Lorito N, Bacci M, Subbiani A, Bonechi F, Comito G, *et al*. Estrogen-dependent activation of TRX2 reverses oxidative stress and metabolic dysfunction associated with steatotic disease. Cell Death Dis 2025;16(1):57. DOI: 10.1038/s41419-025-07331-7, PMID: 39890799.

[28] Klinge CM. Estrogenic control of mitochondrial function. Redox Biol 2020;31:101435. DOI: 10.1016/j.redox.2020.101435, PMID: 32001259.

[29] Wang YL, Wu J, Li RX, Sun YT, Ma YJ, Zhao CY, *et al*. A double-edged sword: The Kelch-like ECH-associated protein 1-nuclear factor erythroid-derived 2-related factor 2-antioxidant response element pathway targeted pharmacological modulation in nonalcoholic fatty liver disease. Curr Opin Pharmacol 2021;60:281–290. DOI: 10.1016/j.coph.2021.07.021, PMID: 34500407.

[30] Calle X, Garrido-Moreno V, Becerra B, Troncoso MF, Silva-Agüero JF, Guajardo-Correa E, *et al*. 17-beta estradiol prevents cardiac myocyte hypertrophy by regulating mitochondrial E3 ubiquitin ligase 1. Cell Death Dis 2025;16(1):111. DOI: 10.1038/s41419-025-07389-3, PMID: 39971924.

[31] Grimm A, Riou A, Gaillard C, Broeglin A, Ureshino RP, Dion V, *et al*. Estetrol Enhances Mitochondrial Bioenergetics and Neurite Outgrowth in Cellular Models of Alzheimer's Disease. Cells 2026; 15(5):452. DOI: 10.3390/cells15050452, PMID: 41827885.

[32] Chen Q, Ruan D, Shi J, Du D, Bian C. The multifaceted roles of natural products in mitochondrial dysfunction. Front Pharmacol 2023;14:1093038. DOI: 10.3389/fphar.2023.1093038, PMID: 36860298.

[33] Huang X, Huang J, Zhang L, Zhu Y, Li Y. A novel ERα-mediated reporter gene assay for screening estrogenic/antiestrogenic chemicals based on LLC-MK2 cells. Toxicol Mech Methods 2014; 24(9):627–632. DOI: 10.3109/15376516.2014.945107, PMID: 25045971.